Room temperature mechanosynthesis of the $La_{1-x}Sr_xMnO_{3\pm\delta}$ ($0\leq x\leq 1$) system and microstructural study

M.J. Sayagués, J.M. Córdoba and F.J. Gotor*

Instituto de Ciencia de Materiales de Sevilla, Centro mixto CSIC-US, Av. Américo Vespucio 49, 41092 Seville, Spain.

Abstract

Monophase nanocrystalline powders belonging to the $\mathbf{La_{1-x}Sr_xMnO_{3\pm\delta}}$ system ($0\leq x\leq 1$) with a perovskite structure have been obtained by mechanochemistry synthesis using a planetary ball milling equipment from La_2O_3, SrO, and Mn_2O_3 mixtures. The solid state reaction was complete after one hour of milling treatment. For all the compositional range, the diffraction domain was very small and the structure appeared as a pseudo cubic perovskite. After annealing at 1100°C under static air, the symmetry evolution due to the La substitution by Sr was analyzed by x-ray and electron diffraction. Samples with x = 0, 0.25, 0.5, and 0.75 were assigned to ***R-3c*** space group (167) in the rhombohedral system and perovskite structure. However, the symmetry of the last term of the system (x=1), $SrMnO_{3\pm\delta}$ sample, changed to ***$P6_3/mmc$*** space group (194) in the hexagonal system. The terms with x = 0.8, 0.85, and 0.9 presented mainly rhombohedral symmetry.

Keywords

Mechanochemistry, Perovskite structure, Microstructural characterization.

* Corresponding author: *sayagues@cica.es*

1. Introduction

The perovskite structure oxides have been widely investigated during the last sixty years [1, 2] and they have special relevance regarding their applications, using their electric, magnetic, and catalytic properties among others [3,4]. In the last fifteen years they have been studied as components for solid oxide fuel cells (SOFCs) [5, 6]. They have been synthesized using several techniques, from the most common and ancient method -as the ceramic [7] -to the newer and sophisticated ones–as the hydrazine method [8] or the combustion synthesis [9].

Solid solutions based on lanthanum strontium manganites $La_{1-x}Sr_xMnO_{3\pm\delta}$ (LSM) are promising materials for oxygen cathodic electrodes [10-19] and it is well known that its final properties depend on the La/Sr ratio as well as on the oxygen stoichiometry [20, 21]. However, the cathode microstructure is also a critical factor in determining the activity and is controlled by several synthesis variables. Thus, the particle size of electrode materials, the heating condition for electrode adhesion, and the cell operation conditions must be considered. J.H. Choi et al. [22] have shown that higher activity is expected with smaller particle sizes and a higher porosity. Because the smaller particles are, however, more vulnerable to sintering under the high temperature electrode adhesion and cell operation conditions, their use can not always guarantee a higher activity. Particle growth leads to a loss of active sites. A trade-off is thus expected at a certain range of particle size between the two conflicting factors, namely, the number of active sites and particle sintering.

This LSM system has been synthesized by several techniques [11-23]; however there are very few works [24-29] regarding their synthesis by mechanochemical method. Zhang et al. have synthesized $LaMnO_3$ and $La_{0.7}Sr_{0.3}MnO_3$ after 3 hours of milling, and Bolarín and co-workers have studied the mechanosynthesis of calcium

doped lanthanum manganites, however the long milling times used, 10 and 20 hours, could introduce high quantity of grinding media impurities.

The aim of this study is to synthesize by a very simple method (**one** hour using a planetary ball milling equipment at room temperature) eight phases belonging to the system $La_{1-x}Sr_xMnO_{3\pm\delta}$ (x=0, 0.25, 0.5, 0.75, 0.80, 085, 0.90, and 1) and analyze the structure before and after annealing at 1100º C in static air. The evaluation of how the x value affects the final structure and symmetry, and how far- in terms of the x value- the solid solution is kept were considered.

2. Materials and methods

Powders of $La_{1-x}Sr_xMnO_{3\pm\delta}$ ($0\leq x\leq 1$) were prepared using a mechanochemical method from stoichiometric amounts of La_2O_3, SrO, and Mn_2O_3 according to the following reaction:

$$\textit{(1-x)/2}\mathbf{La_2O_3} + x\mathbf{SrO} + \textit{1/2}\mathbf{Mn_2O_3} \longrightarrow \mathbf{La_{1-x}Sr_xMnO_{3\pm\delta}}$$

Strontium carbonate (Panreac, 98% in purity), lanthanum oxide (Fluka, 99.98% in purity) and manganese (III) oxide (Aldrich, 99% in purity) powders were used as starting reactants. The $SrCO_3$ was first heated at 1100º C to obtain the SrO.

For each experiment, seven WC balls together with stoichiometric quantities of powder reactants (to get 2 g of the perovskite sample) were placed in a tempered steel vial (67Rc) and milled in a planetary ball mill (model Micro-Mill Pulverisette 7, Fritsch) at a spinning rate of 600 rpm. The volume of the vial was 45 ml. The diameter and weight of the balls were 15 mm and 26.4 g, respectively. The powder to-ball mass ratio (PBR) was approximately 1:92.

The milled powder samples (**M**) were heated (**H**) at 1100º C under static air during 12 hours using a chamber furnace with a heating rate of 10ºC/min and free cooling.

The X-ray diffraction (XRD) patterns of all the samples (**M** and **H**) were obtained in a Panalitycal X'Pert Pro instrument equipped with a goniometer using Cu K radiation (45 kV, 40 mA), a secondary K filter, and an X'Celerator detector. The diffraction patterns were scanned from 20◦ to 150◦ (2θ) at a scanning rate of 0.0037◦ min^{-1}. Lattice parameters of samples were calculated from the whole set of peaks of the XRD diagram using the FullProf free-software in a profile matching mode [30] .

High-temperature X-ray powder diffraction diagrams were recorded on the previous mentioned instrument, which was equipped with an Anton Parr high-temperature attachment (HTK 1200). The diffraction diagrams were obtained under air atmosphere at temperature intervals of 100 °C (up and down), and a maximum temperature of 1100 °C was investigated. The heating rate was set to 5 °C/min, and a scanning rate of 5.4°min^{-1} was applied. In total, the 2θ range was scanned from 20° to 70° for 12 min and 18 s.

Thermogravimetric measurements were performed by means of a TGA equipment developed on the basis of a CI Robal electrobalance (C.I. Electronics Ltd.) attached to the support frame of a high-temperature vertical furnace (1500 ºC; Severn Furnaces Ltd.) and connected to a system of flowing gases up to a total pressure of 1 atm. Samples were placed into an alumina crucible, which was centered inside an 8 mm inner diameter ceramic tube in order to minimize the buoyancy. The absolute oxygen content was determined by reducing the samples under a reductive mixture atmosphere of He/H_2 (1/1 ratio) controlled by a digital rotametter system. A heating rate of 10 °C/min from room temperature to 1200 °C was used and maintained the time required

to ensure complete reduction. The total weight loss was recorded and oxygen content was calculated taking into account that $La_{1-x}Sr_xMnO_{3\pm\delta}$ samples were reduced to a mixture of oxides where the lanthanum, strontium, and manganese oxidation states are ***3+***, ***2+***, and ***2+***, respectively.

Microstructural characterization was carried out by using scanning and transmission electron microscopy (SEM and TEM) techniques. Powder samples were dispersed in acetone and droplets of the suspension were deposited onto a holey C film. The SEM images were obtained on a Hitachi S-4800 SEM-FEG microscope. Transmission electron microscopy (TEM) images and electron diffraction (ED) patterns were taken on a 200 kV Philips CM200 microscope equipped with a supertwin objective lens and a LaB_6 filament (point resolution ∅ = 0.25 nm).

3. Results and discussion

A first set of experiments was conducted for the x=0.25 composition ($La_{0.75}Sr_{0.25}MnO_{3\pm\delta}$, **M2** sample) to determine the optimum milling time to complete the solid state reaction under the conditions described above. The products obtained at increasing time were analyzed by x-ray diffraction and the results are presented in figure 1. It is easy to observe how the reaction progressed significantly after 15 minutes of milling and after half an hour was nearly finished. After only 45 minutes, no reactant peaks were detected and the solid state reaction seemed to be complete.

To be sure of achieving full conversion, the mechanochemical synthesis of the powder samples was then carried out using one hour of milling. Figure 2 shows the difractograms corresponding to the eight samples belonging to the $La_{1-x}Sr_xMnO_{3\pm\delta}$ ($0\leq x\leq 1$) system (**M** samples). All of them present a single phase with pseudo-cubic symmetry and perovskite structure. The shift observed in the XRD reflections was

attributed to different La and Sr ratio in the pseudo-cubic structure. In the inset of figure 2a (x=0, 0.25, 0.5 and 0.75) can be observed a clear displacement to smaller *d* spacing when x value increases. However in the inset of figure 2b can be appreciated that the peak displacement is not so clear, probably due to the small x discrepancy (x=0.8, 0.85, 0.9 and 1).

Fullprof computer program was used from the whole set of peaks of the XRD patterns (Fig. 2a and b) to calculate unit cell dimensions for each phase in the system, assuming (pseudo) cubic unit cell, the found results and the average crystallite sizes (D) are presented in table I, the cell parameters decreased with increasing substitution of La by Sr. As can be deduced from the large broadening of reflections in figure 2 the crystalline domain is very small, around 20 nm, it can be corroborated in the SEM and TEM micrographs showed below (Fig. 7 and 8). ,

The X-ray diffraction diagrams of powder samples treated at 1100°C under air atmosphere are presented in figure 3 (**H** samples). It is clear that a higher crystallinity and a well defined symmetry took place. As observed in the **M** samples, the XRD reflections are shifted to smaller d-spacing as a consequence of the La substitution, which is very clear from x=0 to x=0.8, according with the cell parameters. For samples with x=0 and 0.25, some of the maxima are clearly split showing a structure very similar to $La_{0.95}Mn_{0.95}O_3$ (reference pattern-01085-1838) calculated by Van Roosmalen et al [31] with rhombohedral cell (***R-3c***, 167 space group). However, the diffraction lines (enlarged in the inset for the main one) for samples with x=0.5, 0.75, 0.8, 0.85, and 0.9 were not split that could be due to a different symmetry or different lattice parameter and same symmetry. To elucidate this feature and calculate the lattice parameters the Fullprof computer program was used from the whole set of peaks of the XRD diagram, assuming a rhombohedral symmetry or cubic structure. The results showed a better fit

when rhombohedral symmetry (***R-3c*** space group) was used (table I) for samples in the range of $0 \leq x \leq 0.90$. Nevertheless, when the x value is equal to one ($SrMnO_3$), another perovskite structure with hexagonal symmetry and ***$P6_3/mmc$*** space group (194) was observed. This term is excluded from the $La_{1-x}Sr_xMnO_{3\pm\delta}$ solid solution as the symmetry and cell parameters change, being ***a*** very similar but ***c*** smaller with respect to the rhombohedral structure.

Results in table I show how substitution of La by Sr modifies the lattice parameters of the rhombohedral structure in such a way that the volume of the unit cell decreases with the *x* value. This trend was observed in both **M** and **H** samples as shown in figure 4. The term x=1 is not presented as not belong to the rhombohedral solid solution. The volume diminution is due to the Mn^{4+} formation at the same time that La^{3+} is substitute by Sr^{2+} in the cationic subcell for keeping electroneutrality. This is consistent with the fact that the ionic radius of Mn^{4+} (53 pm) is smaller than that of Mn^{3+} (65 pm), and indicates that the manganese ionic radius is in fact the determinant of the unit cell volume. This is significant since La^{3+} (136 pm) has a smaller ionic radius compared with Sr^{2+} (144 pm). The ionic radius values are taken from Shannon considering the coordination number for each cation in the perovskite structure [32]. Moreover, it is worth noting that the presence of Mn^{4+}, which increases with increasing strontium content, reduces the John-Teller effect that was favoured by the Mn^{3+} cation. This fact can explain the absence of the splitting of XRD peaks when the x values increase because of a higher symmetry of the structure. The intensity of some peaks in the difractogram is as also changing with the La substitution. The intensity is decreasing with the increasing Sr quantity. This effect is appreciated very clearly in the first peak which correspond to (012) from the rhombohedral cell (marked in the figure 3a), which corresponds to (100) in the pseudocubic cell, where the La and Sr atoms are located.

To quantify the oxygen composition (delta value) and the oxidation state of the manganese (% Mn^{4+}), thermogravimetric analysis were performed in all the heated samples (**H**). All the results are presented in table I and figure 5. It was found that the amount of Mn^{4+} increased linearly with Sr^{2+} to reach the electroneutrality in the structure, while the oxygen stoichiometry approached to the value of three.

With the purpose of studying the crystallization and symmetry change of milled samples (**M** pseudocubic symmetry) after annealing (**H** rhombohedral symmetry), experimental XRD measurements as a function of the temperature (up and down) under air atmosphere were carried out. XRD difractograms every 100°C, from 30°C till 1100°C and vice versa were recorded. A summary of the obtained results are presented in figure 6 corresponding to M2 sample. When the experiment rises in temperature crystallization process could be observed and at 1100°C a small peak (aprox. $2\theta=35^{o}$, marked with an asterisk) appears -which could be due to a formation of an orthorhombic phase [33]-. Lowering down in temperature the small peak stays till 800°C and below this temperature disappears. Below 500°C some of the reflexions start to split (see inset of figure 6) and a small peak before $2\theta=40^{o}$ appears (marked with a cross), indicating the formation of the rhombohedral phase. This fact indicates that the rhombohedral phase stabilizes at low temperature and can be explained in terms of oxygen composition. The orthorhombic phase stable at high temperature (1100°C) its able to accommodate less quantity of oxygen in the structure [33] than the rhombohedral one, that stabilize below 500°C with an oxygen composition of. $La_{0.75}Sr_{0.25}MnO_{3.11}$ (see table I)

The microcharacterization of **M** and **H** samples were analyzed by SEM, TEM and ED techniques. Figure 7 presents the SEM micrographs found for some of the milled and heated materials, which are representative of the obtained results. All **M** samples

(pseudocubic perovskite structure) had a similar microstructure characterized by aggregates of small particles. As expected, **H** samples were composed of larger faceted particles, being very similar in shape as can be seen in **H1** and **H2** (same rhombohedral symmetry); however **H8** sample (with a different symmetry, hexagonal) presented very round particles and smaller in size.

Figure 8 shows the TEM and ED representative results of the **M** and **H** samples. The TEM micrograph corresponding to **M1** sample (x=0) showed quite large particles formed in fact by agglomerated small crystallites in the nanometric range (Fig.8a) as evidenced by the presence of rings in the ED pattern. All the rings could be indexed in the pseudocubic structure (***Pm-3m***). TEM micrographs of **H1** (fig. 8b) and **H3** (fig. 8c) samples also showed the presence of aggregates but formed by submicrometric crystallites of several hundred nanometers as observed in the enlargements of two of these crystals. The corresponding EDPs were taken along the [001], [211] and [210] zone axis. All maxima could be indexed in the rhombohedral structure (***R-3c***).

The TEM results corresponding to **H8** sample (x=1) are presented in fig 8d, which shows an image where crystals with different sizes can be appreciated. All the found ED could be indexed in the hexagonal structure (***P6$_3$/mmc***) confirming the XRD results. The ED pattern presented was taken along the [201] zone axes.

4. Conclusions

Mechanochemical method is a good alternative to synthesize phases with perovskite structure belonging to the $La_{1-x}Sr_xMnO_{3\pm\delta}$ system, which is a proper candidate for cathodes in SOFCs. The rhombohedral phase (***R-3c***), found after annealing the **M** samples, is kept along the solid solution in the range of $0 \leq x \leq 0.90$ and is a low temperature stable phase, nevertheless when x=1 ($SrMnO_3$), appears

another perovskite structure with hexagonal symmetry and ***P6$_3$/mmc*** space group (194). From XRD data, it could be observed that the Sr substitution has influence on the cell parameters, and the volume decreases when x increases. Although La^{3+} (136 pm) has a smaller ionic radius than Sr^{2+} (144 pm), Sr substitution implies Mn^{4+} formation, which is smaller (53 pm) than Mn^{3+} (65 pm).

The microstuctural characterization showed that the powder samples after mechanical milling have nanometer character. After the temperature treatment the crystallite size increases, but is still quite small and suitable for the future application.

Acknowledgement

This work was supported by the Spanish government under grant No. MAT2010-17046 that was financed in part by the European Regional Development Fund 2007-2013. J. M. Córdoba was supported by CSIC through JAE-Doc grant, financed in part by the European Social Fund (ESF). The authors wish to thank Ms. C. Gallardo for her assistance in high-energy ball-milling experiments.

References

[1] A.S. Bhalla, Ruyan Guo and Rustum Roy. Mat Res Innovat 4 (2000) 3-26.

[2] M. A. Peña and J.L.G. Fierro. J. Chem Rev J. Nansci. Nanotech. 101 (2001) 1981-2017.

[3] D. Dimos, and C.H. Mueller. Annual Review of Mater. Sci. 28 (1998) 397-419.

[4] B. Raveau, A. Maignan, C. Martin and M Hervieu, Chem. Mater. 10 (1998) 2641-2652.

[5] A. J. Jacobson, Chem. Mater. 22 (2010) 660-674.

[6] A. Orera and P. R. Slater, Chem. Mater. 22 (2010) 675-690.

[7] R. Chiba, F. Yoshimura and Y. Sakurai, Solid State Ionics 152-153 (2002) 575-582.

[8] K. Azegami, M. Yoshinaka, K. Hirota and O. Yamaguchi, Mater. Res. Bull. 33(2) (1998) 341-348.

[9] N. P. Bansal and Z. Zhong, J. Power Sources 158 (2006) 148-153.

[10] J. Van Herle, A. J. McEvov and K. Ravindranathan Thampi. Electrochem. Acta 41(9**)** (1996) 1447-1454.

[11] E. P. Murray, T. Tasai and S. A. Barnett, Solid State Ionics 110 (1998) 235-243.

[12] C. M. D'Souza and N. M. Sammes, J. Am. Ceram. Soc. 83(1) (2000) 47-52.

[13] J.Q. Li and P. Xiao. J. Eur. Cer. Soc. 21 (2001) 659-668.

[14] D. L. Meixner and R. A. Cutler, Solid State Ionics 146 (2002) 273-284.

[15] S. Kocha, P. Vang Hendriksen, T. Jacobsenb and L. Bay, Solid State Ionics, 176 (2005) 861-869.

[16] Anne C., Co and Viola I. Birss, J. Phys. Chem. B, 110 (2006) 11299-11309.

[17] R. Tiana, J. Fana, Y. Liu and C. Xia, J. Power Sources, 185 (2008) 1247-1251.

[18] B. P. McCarthy, L. R. Pederson, R. E. Williford, and X. Zhou, J. Am. Ceram. Soc., 92(8) (2009) 1672-1678.

[19] J. R. Wilson, A. T. Duong., M. Gameiro., H. Chen, K. Thornton, D. R. Mummb and, S. A. Barnett. Electrochem. Comm., 11 (2009) 1052-1056.

[20] M. J. L. Ostergard, C. Clausen, C. bagger and M. Mogensen, Electrochimica Acta 40(12) (1995) 1971-1981.

[21] S. Tanasescu, N.D. Totir, D.I. Marchidan and A. Turkanu, Mat. Res. Bull. 32(7) (1997) 915-923.

[22] J. H. Choi, J. H. Jang, J. H. Ryu, S. M. Oh, J. Power Sources 87 (2000) 92-100.

[23] M. Gaudona, C. Laberty-Robert, F. Ansart, L. Dessemond and P. Stevens, J. Power Sources 133 (2004) 214–222.

[24] Q. Zhang, T. Nakagawa and F. Saito, J. Alloys & Comp. 308 1(2000) 21-125.

[25] Q. Zhang and F. Saito, J. Alloys & Comp. 297 (2000) 99-103.

[26] J. Chaichanawong, K. Sato1, H. Abe, K. Murata, T. Fukui, T. Charinpanitkul, W.Tanthapanichakoon and M. Naito, Advanced Powder Technol. 17(6) (2006) 613-622.

[27] A.M. Bolarín , F. Sánchez , S. Palomares, J.A. Aguilar, G. Torres-Villaseñor, J. Alloys & Comp. 436 (2007) 335–340.

[28] A.M. Bolarín F. Sánchez, A. Ponce, E.E. Martínez, Materials Science and Engineering A, 454–455 (2007) 69-74.

[29] I. A. Lira-Hernández, F. Sánchez-De Jesús, C. A. Cortés-Escobedo, and A. M. Bolarín-Miro, J. Am. Ceram. Soc., 93 [10] (2010) 3474-3477.

[30] J. Rodriguez-Carvajal. Newsletter, 26 (2001) 12–19.

[31] J.A.M. Van Roosmalen, E.H.P. Cordfunke, R.B. Helmholdt, H.W. Zandbergen. J. Solid State Chem. 110 (1994) 100-105.

[32] R.D. Shannon. Acta Cryst. A32: (1976) 751-767.

[33] M. Paraskevopoulos, F. Mayr, C. Hartinger, A. Pimenov, J. Hemberger, P. Lunkenheimer, A. Loidl, A.A. Mukhin, V.Yu. Ivanov, A.M. Balbashov, Journal of Magnetism and Magnetic Materials, 21**1** (2000) 118-127.

Figure captions

Figure 1. Time evolution by X-ray diffraction of the solid state reaction to synthesize $La_{1-x}Sr_xMnO_{3\pm\delta}$ (x=0.25) sample by mechanochemistry.

Figure 2. X-ray diffraction diagrams corresponding to the $La_{1-x}Sr_xMnO_{3\pm\delta}$ system (a) x=0, 0.25, 0.50 and 0.75, and (b) x=0.80, 0.85, 0.90 and 1, obtained by mechanochemical synthesis (**M** samples). The inset shows an enlargement of the highest maxima to reveal the displacement in the *d* spacing due to the La substitution.

Figure 3. X-ray diffraction diagrams corresponding to the heated samples (**H**) at 1100°C under air, belonging to the $La_{1-x}Sr_xMnO_{3\pm\delta}$ system (a) x=0, 0.25, 0.50, and 0.75 and (b) x=0.80, 0.85, 0.90 and 1. The inset shows an enlargement of the highest maxima.

Figure 4. Unit cell volume variation with x value in the $La_{1-x}Sr_xMnO_{3\pm\delta}$ system. (a) **M** samples and (b) **H** Samples.

Figure 5. (a) Oxygen stoichiometry (delta value) and (b) Mn^{4+} content (%) versus x, in the $La_{1-x}Sr_xMnO_{3\pm\delta}$ system for **H** Samples.

Figure 6. Thermal evolution of the XRD diagram of **M2** sample ($La_{0.75}Sr_{0.25}MnO_{3\pm\delta}$) under air atmosphere from 30°C to 1100°C and vice versa from 1100°C to 30°C. The inset shows an enlargement of the highest maxima.

Figure 7. SEM micrographs corresponding to samples **M1** and **H1**(x=0), **M2** and **H2** (x=0.25) and **M8** and **H8** (x=1).

Figure 8. TEM micrographs and ED patterns corresponding to **M1** (a), **H1** (b), **H3** (c) and **H8** (d) samples.

Table I. Structural and chemical parameters for all the synthesized samples in the $La_{1x}Sr_xMnO_{3\pm\delta}$ system, in the first step after milling (**M** samples) and after heated at 1100 °C under air atmosphere during 12 hours (**H** samples).

Sample	**Compound**	***a* (Å)**	***c* (Å)**	**D (nm)**	**Mn^{4+} (%)**	**δ value**
(x=0)	$LaMnO_{3\pm\delta}$					
M1	(Pm-3m)	3.9114		16		
H1	(R-3c)	5.5306	13.5668	88	34%	0.17
(x=0.25)	$La_{0.75}Sr_{0.25}MnO_{3\pm\delta}$					
M2	(Pm-3m)	3.9013		23		
H2	(R-3c)	5.5237	13.3790	176	47%	0.11
(x=0. 5)	$La_{0.5}Sr_{0.5}MnO_{3\pm\delta}$					
M3	(Pm-3m)	3.8883		22		
H3	(R-3c)	5.4499	13.3799	88	74 %	0.07
(x=0.75)	$La_{0.25}Sr_{0.75}MnO_{3\pm\delta}$					
M4	(Pm-3m)	3.8686		16		
H4	(R-3c)	5.4353	13.3120	110	79%	0.02
(x=0.80)	$La_{0.20}Sr_{0.80}MnO_{3\pm\delta}$					
M5	(Pm-3m)	3.8585		20		
H5	(R-3c)	5.4226	13.3007	38	82%	0.01
(x=0.85)	$La_{0.20}Sr_{0.80}MnO_{3\pm\delta}$					
M6	(Pm-3m)	3.8502		18		
H6	(R-3c)	5.4268	13.3253	56	80%	0.025
(x=0.90)	$La_{0.20}Sr_{0.80}MnO_{3\pm\delta}$					
M7	(Pm-3m)	3.8416		16		
H7	(R-3c)	5.4287	13.2991	61	92%	0.02
(x=1)	$SrMnO_{3\pm\delta}$					
M8	(Pm-3m)	3.8511		21		
H8	(P63/mmc)	5.4572	9.1076	76	100 %	0.00

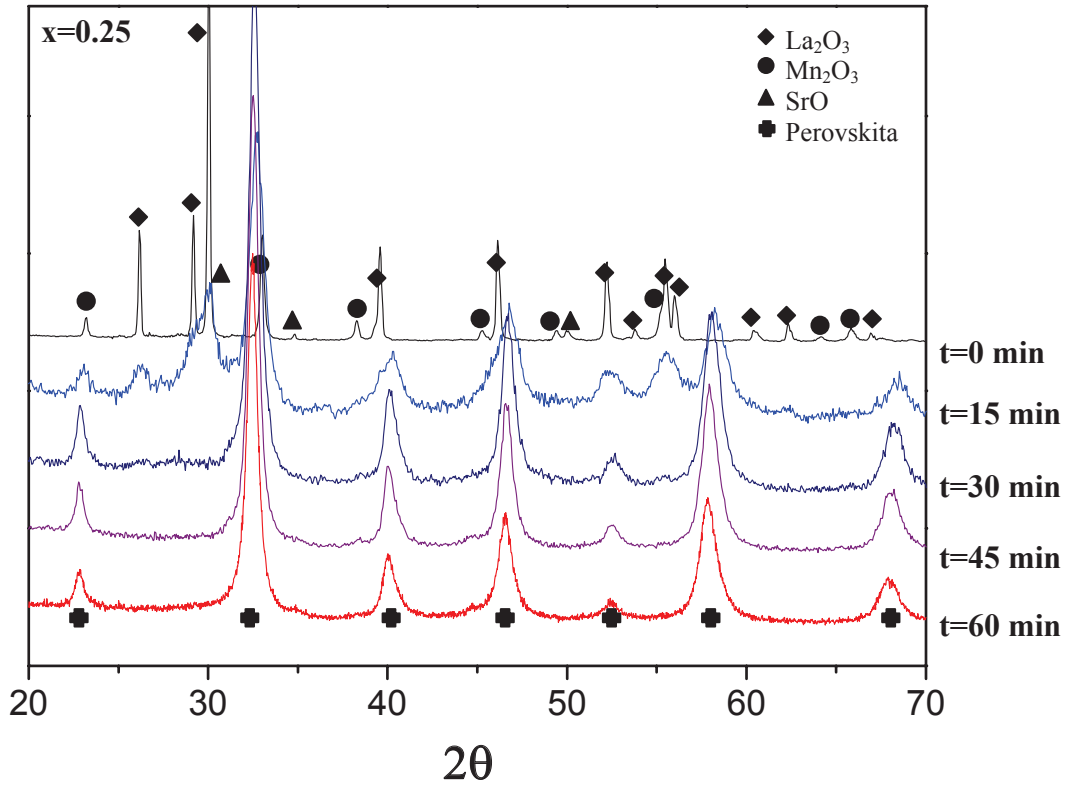
x=0.25
La2O3
Mn2O3
SrO
Perovskita
t=0 min
t=15 min
t=30 min
t=45 min
t=60 min
20
30
40
50
60
70
2θ

Figure 1

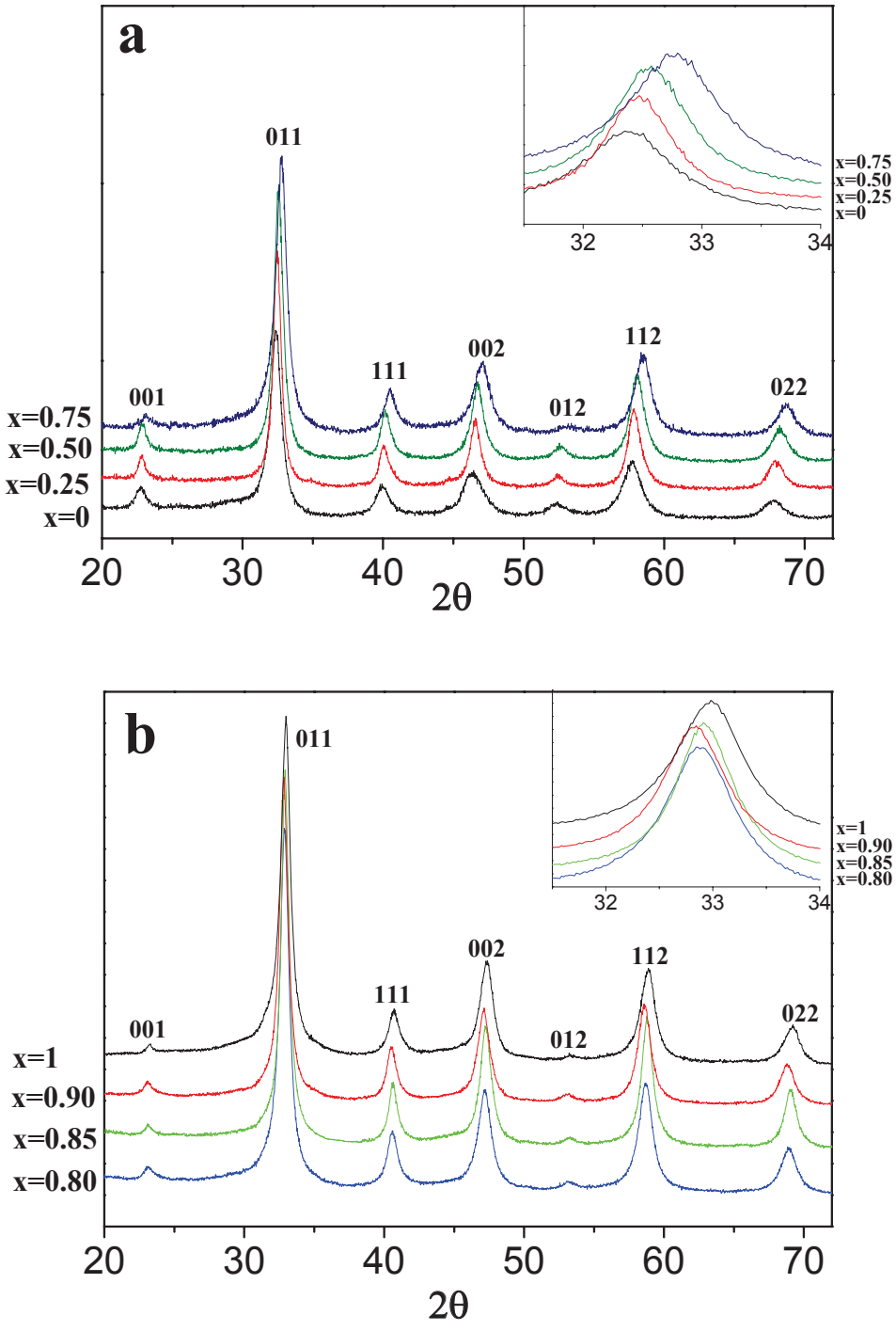
a
011
001
111
002
012
112
022
x=0.75
x=0.50
x=0.25
x=0
20
30
40
50
60
70
2θ
32
33
34
b
011
001
111
002
012
112
022
x=1
x=0.90
x=0.85
x=0.80
20
30
40
50
60
70
2θ
32
33
34

Figure 2

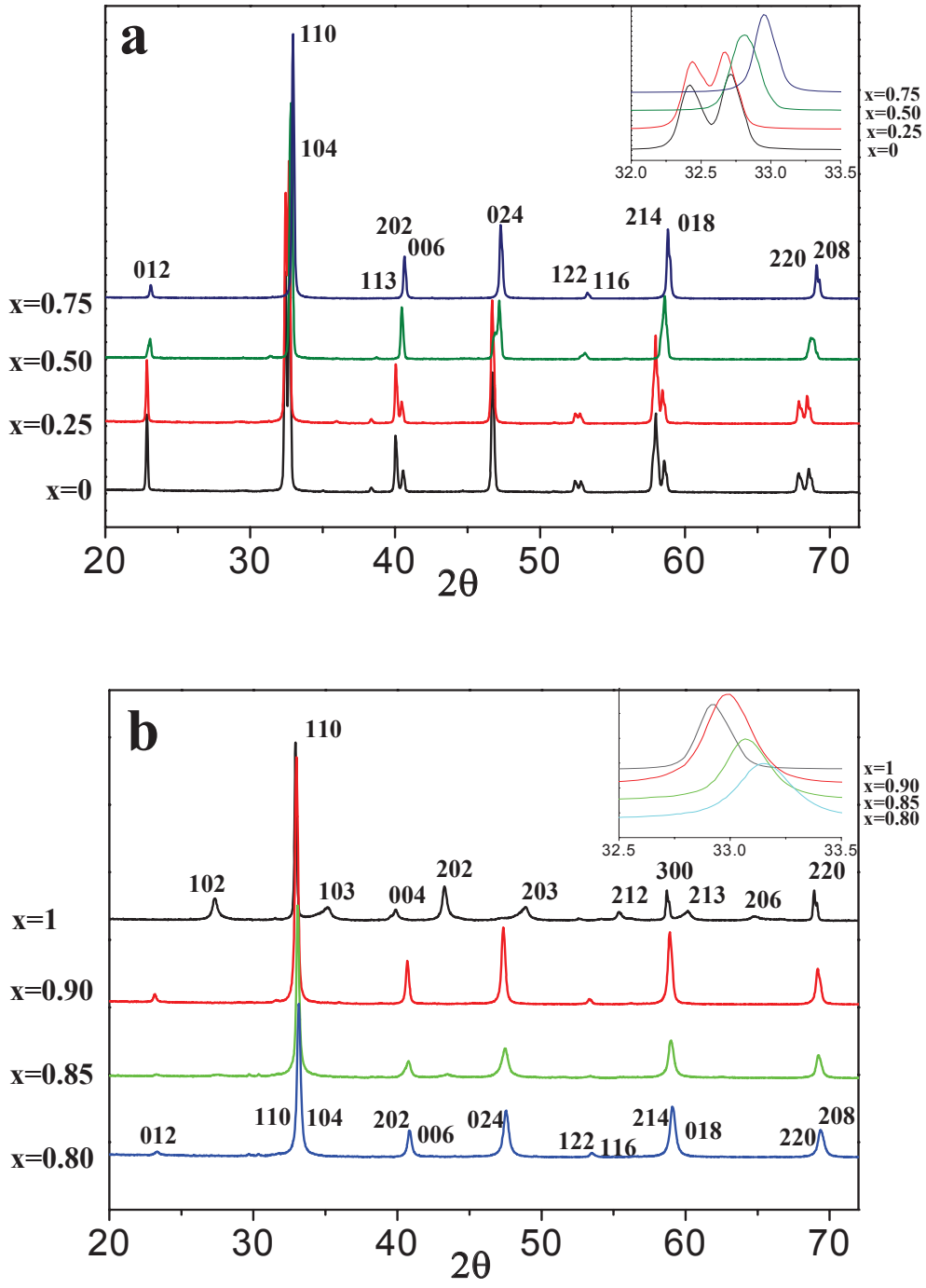
a
110
104
202
006
113
024
122
116
214
018
012
220
208
x=0.75
x=0.50
x=0.25
x=0
20
30
40
50
60
70
2θ
32.0
32.5
33.0
33.5
x=0.75
x=0.50
x=0.25
x=0
b
110
102
103
004
202
203
212
300
213
206
220
x=1
x=0.90
x=0.85
x=0.80
012
110
104
202
006
024
122
116
214
018
220
208
32.5
33.0
33.5
x=1
x=0.90
x=0.85
x=0.80

Figure 3

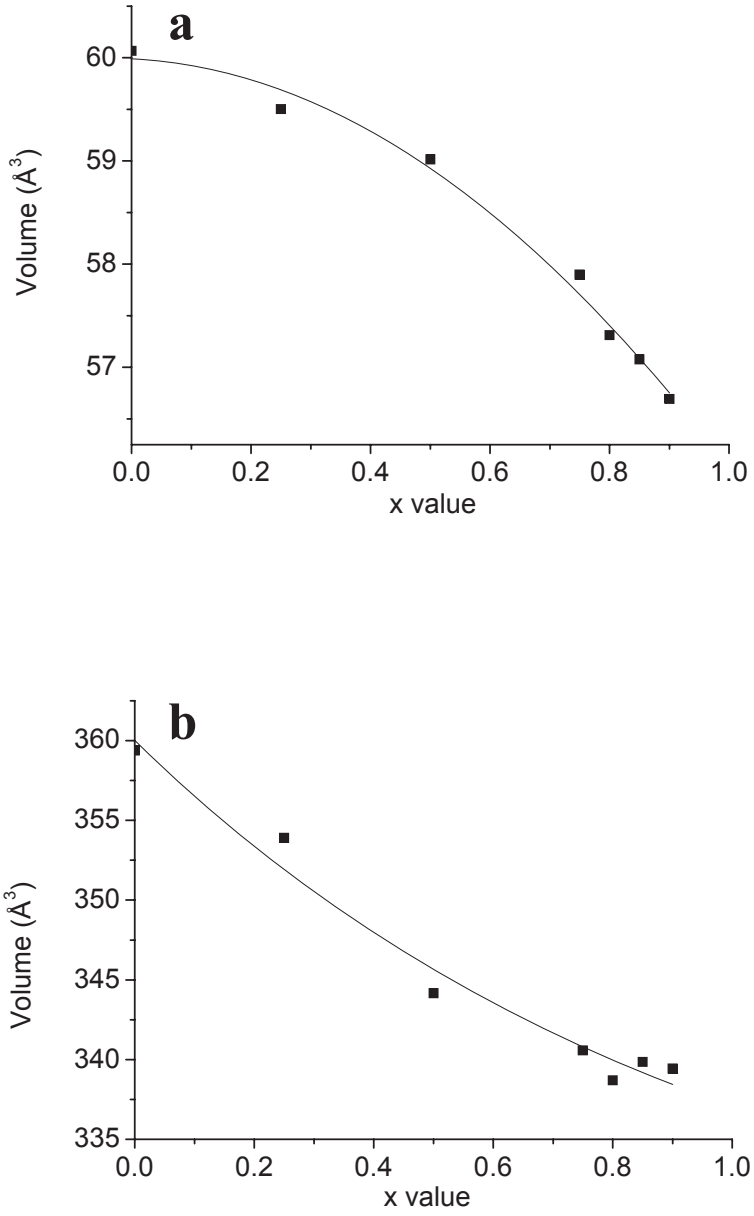
a
60
59
58
57
Volume (Å^3)
0.0
0.2
0.4
0.6
0.8
1.0
x value
b
360
355
350
345
340
335
Volume (Å^3)
0.0
0.2
0.4
0.6
0.8
1.0
x value

Figure 4

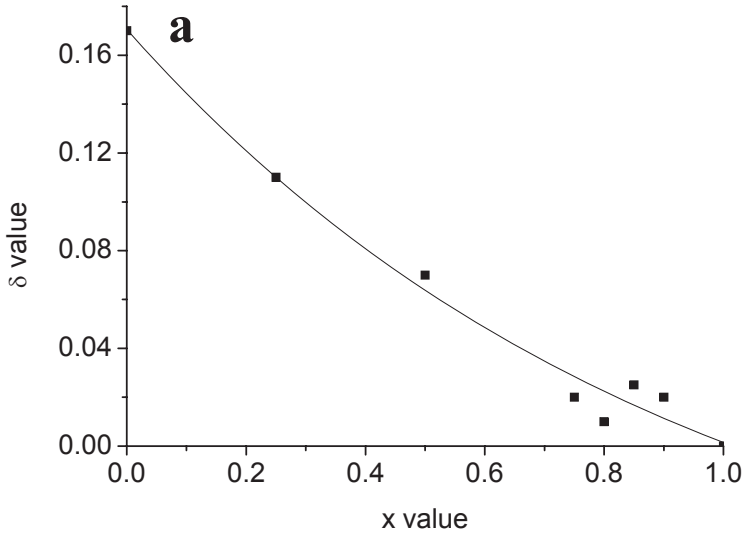
a
0.16
0.12
0.08
0.04
0.00
δ value
0.0
0.2
0.4
0.6
0.8
1.0
x value

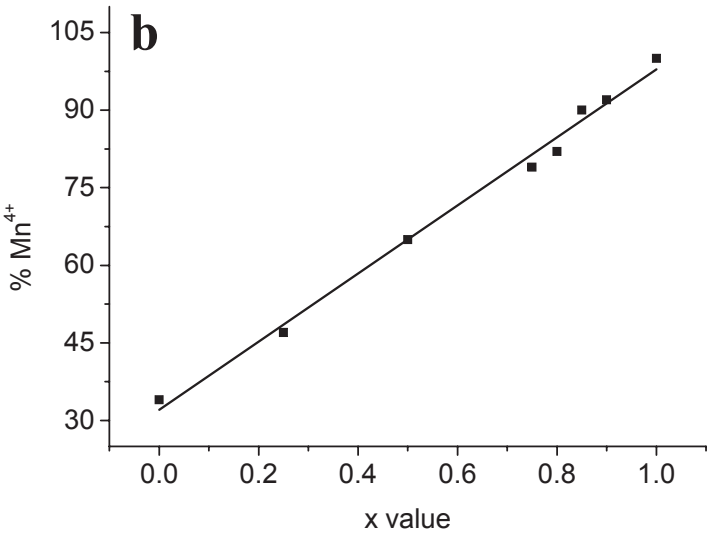
b
105
90
75
60
45
30
% Mn4+
0.0
0.2
0.4
0.6
0.8
1.0
x value

Figure 5

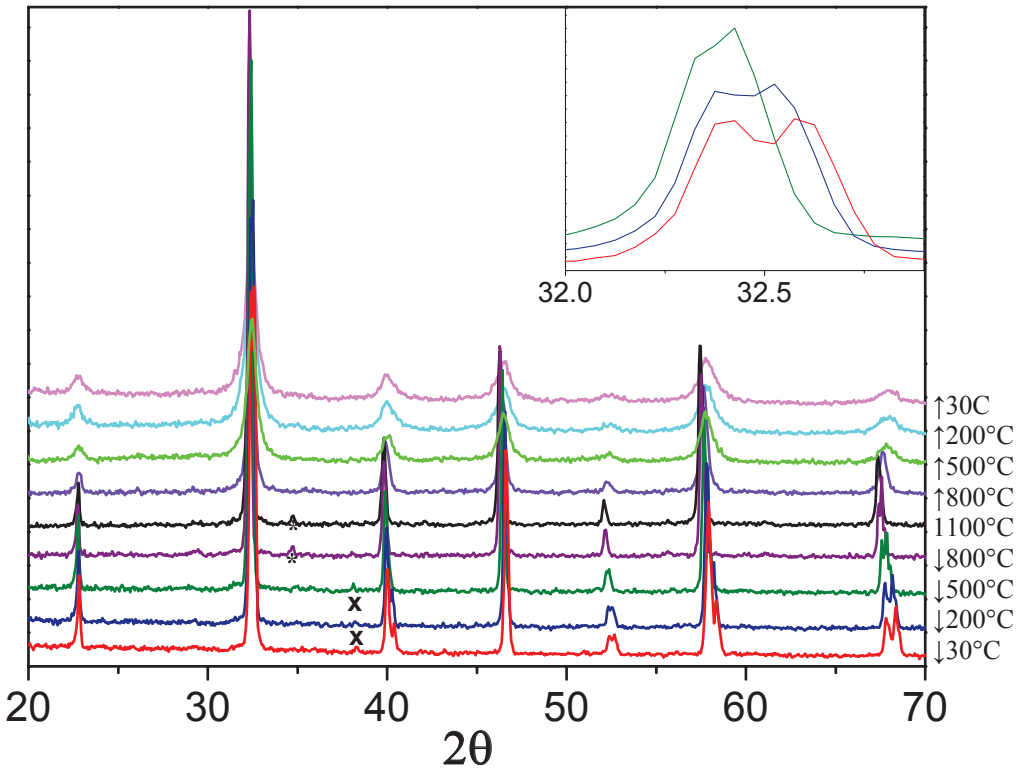
32.0
32.5
↑30C
↑200°C
↑500°C
↑800°C
1100°C
↓800°C
↓500°C
↓200°C
↓30°C
x
x
20
30
40
50
60
70
2θ

Figure 6

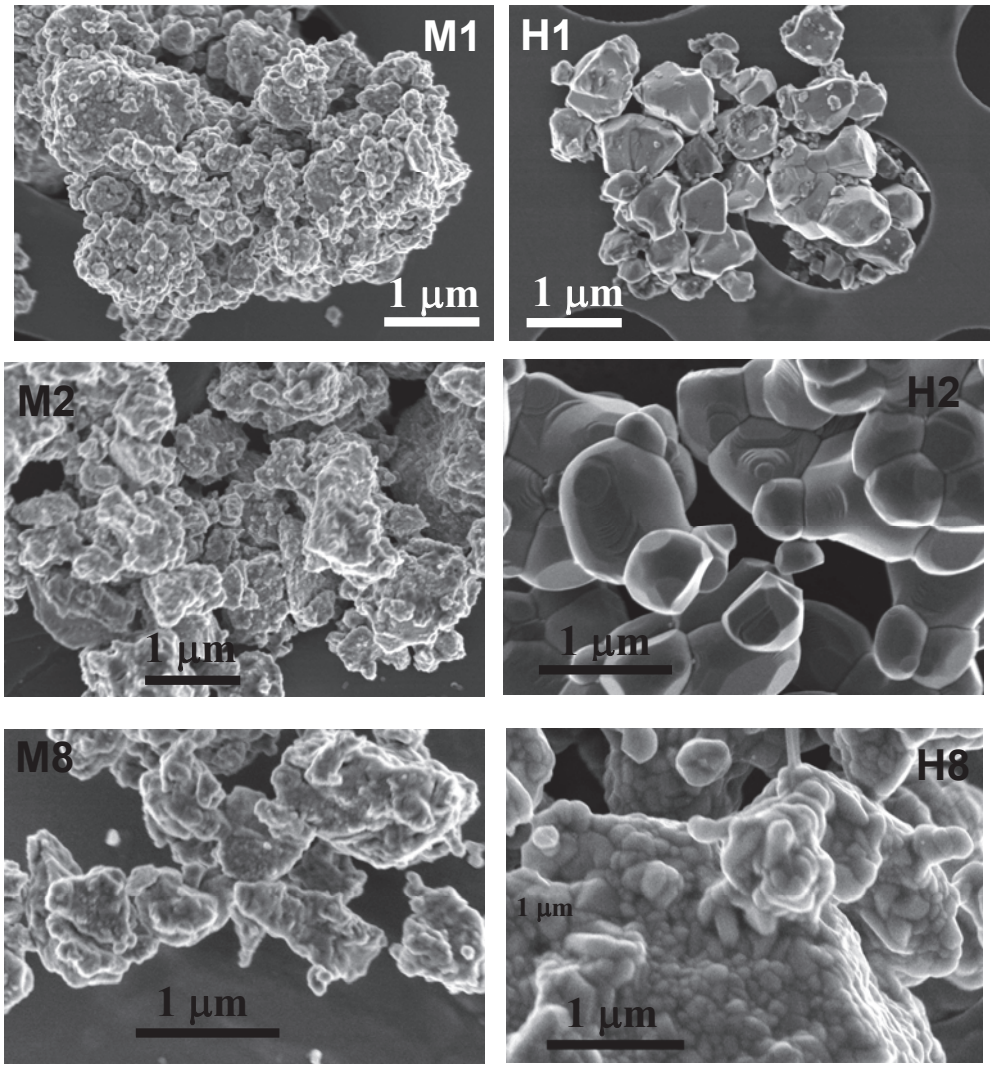

Figure 7

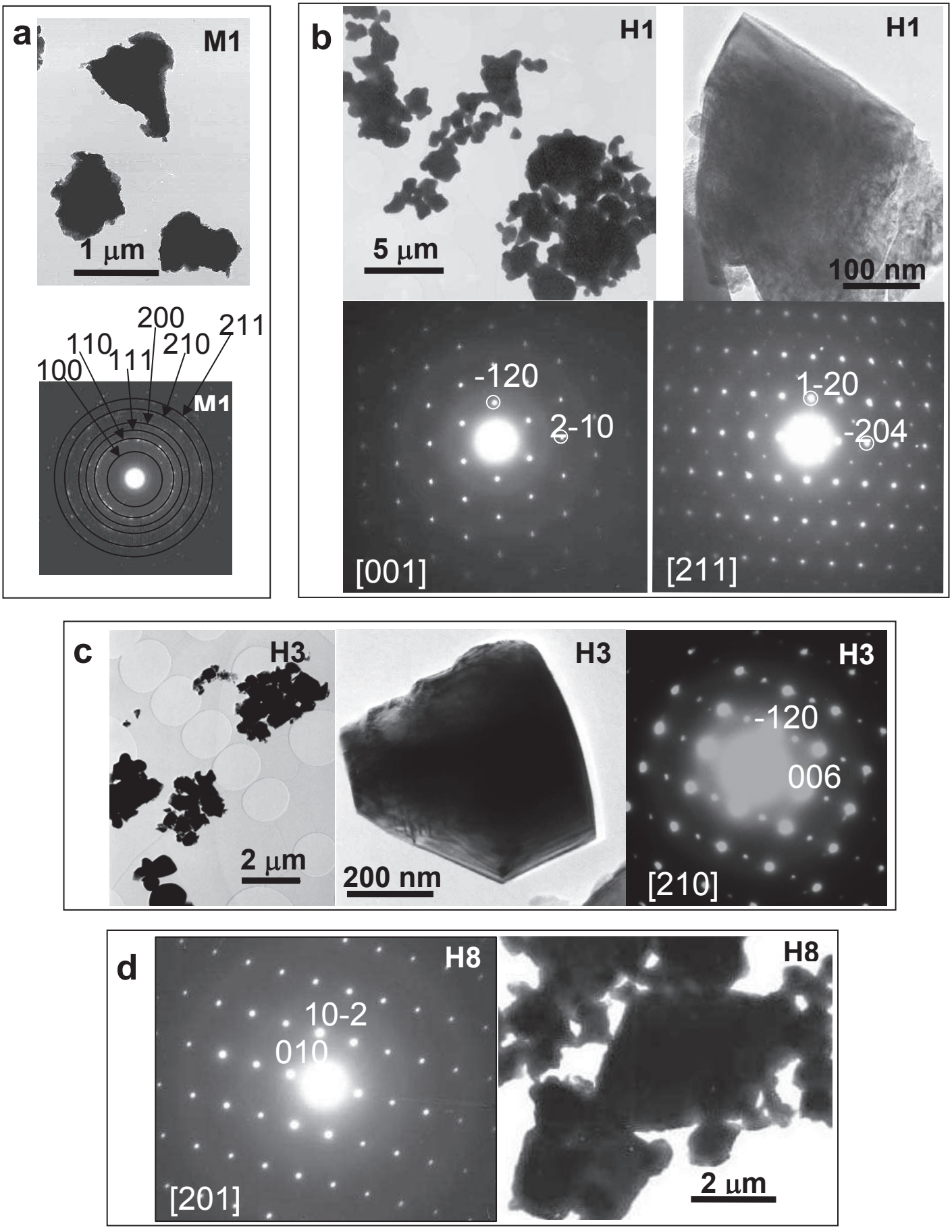
a
M1
1 μm
200
211
110
210
111
100
M1
b
H1
5 μm
H1
100 nm
-120
2-10
[001]
1-20
-204
[211]
c
H3
2 μm
H3
200 nm
H3
-120
006
[210]
d
H8
10-2
010
[201]
H8
2 μm

Figure 8